Theoretical and experimental investigation of the effective g factor of donor-bound electrons in InSb

Z. Barticevic,* M. Dobrowolska, J. K. Furdyna, L. R. Ram Mohan,† and S. Rodriguez
Department of Physics, Purdue University, West Lafayette, Indiana 47907
(Received 27 October 1986)

Spin resonance of donor-bound electrons in n-type InSb is investigated experimentally and theoretically. The resonance is observed in far-infrared magnetotransmission experiments carried out in the wavelength range 96.5—151 μm on a series of samples with various doping levels. That the resonance is due to donor-bound electrons is established unambiguously from the dependence of the resonance intensity on temperature, magnetic field, and donor concentration. Owing to the extremely narrow linewidth of the resonance, the effective g factor of the donor electrons, g_b, can be determined very precisely and can be compared to the g factor of the conduction electrons, g_c. We formulate a theoretical model which predicts the behavior of $g_c - g_b$ in analytical terms. By fitting our experimental data to the model, we then obtain a set of parameters which completely describe the value, magnetic field dependence, and anisotropy of the effective g factor for donor-bound electrons in InSb. The observed anisotropy of g_b is the same as that for g_c. The small difference in the anisotropies of g_b and g_c predicted by the theory is apparently less than the margin of error in our experiment.

I. INTRODUCTION

In InSb the low value of the effective mass—and consequently large effective Bohr radius a^*—is responsible for the small donor binding energies and for the overlap of impurity wave functions which occurs at zero magnetic field even in very pure samples of this material. As a result, the donor energy levels are "smeared out," and merge with the conduction band. As is well known, application of a magnetic field increases the binding energy and reduces the wave-function overlap, which in turn leads to "freezeout" of free carriers, i.e., to electron localization at donor sites. This occurs when the quantity γ, defined by

$$\gamma = \frac{\hbar\omega_c}{2\mathscr{R}^*} , \tag{1}$$

is much larger than unity. Here ω_c is the cyclotron resonance frequency and $\mathscr{R}^*$ the effective Rydberg energy, which for InSb is 0.6 meV. For InSb this limit is typically reached at magnetic fields above 1 T.

The experimentally observed magneto-optical transitions, such as the impurity-shifted cyclotron resonance and the impurity combined resonance,[1–4] are well described by the existing theory.[5] This theoretical formulation does not fully explain the effective g factor associated with the spin resonance of donor-bound electrons. The spin-flip transition of donors in InSb was first reported by McCombe and Wagner[6] and by Appold *et al.*[7]

The purpose of this paper is to present a theory of the g factors for conduction electrons and for electrons bound to donors in zinc-blende semiconductors. The results of the theory are compared with existing experimental data for electric-dipole-excited spin resonance of conduction and donor-bound electrons in n-type InSb, observed in far-infrared (FIR) magnetotransmission. At low temperatures the spin-resonance lines appearing in the FIR transmission spectrum are extremely sharp (the lines are less than 100 G wide at 40 kG so that the resonance position can be pin-pointed within 10 G), allowing a very precise determination of the g factors for both the conduction-band Landau levels and for the Zeeman sublevels of the donor ground state. We shall relate the position of both resonances to a set of phenomenological constants describing the dynamics of the conduction electrons in crystals with the point symmetry group T_d.

The structure of this paper is as follows. In Sec. II we develop a theory of the g factors for electrons in the Γ_6 conduction band, as well as for electrons in the ground state of a donor in a zinc-blend-type semiconductor. In Sec. III we describe the FIR magnetotransmission apparatus and sample preparation. Finally, in Sec. V we present the experimental results and their interpretation.

II. THEORY

In this section we give first a theory of the g factor for electrons in the Γ_6 conduction band of a zinc-blende-type semiconductor. The final expression for the g factors is given in terms of three phenomenological constants. A similar development is subsequently carried out for electrons in the ground state of a donor in the limit $\gamma \gg 1$. This program is carried out because, as we shall see, the g factors for conduction band and bound electrons differ. The difference between these g factors forms the main subject of this paper.

We describe the electrons in the conduction band of a zinc-blende semiconductor using the effective-mass approximation and expand the energy as a function of the wave vector $\mathbf{k}$ to include terms up to fourth powers of the components of the wave vector. The energy eigenvalues

for an electron with wave vector $\mathbf{k}$ are obtained by diagonalizing

$$E(\mathbf{k})=\sum_{\mu}\sigma_{\mu}E_{\mu}(\mathbf{k}) , \tag{2}$$

where μ ranges over the indices $0,x,y,z$; σ_0 is the two-dimensional unit matrix and σ_x, σ_y, and σ_z are the components of the Pauli spin operator with respect to the cubic axes x,y,z. The quantity $E(\mathbf{k})$ and, hence, $E_0(\mathbf{k})$ must belong to the totally symmetric representation of the point group T_d. Since σ_x, σ_y, and σ_z belong to the irreducible representation Γ_4, the quantities $E_x(\mathbf{k})$, $E_y(\mathbf{k})$, and $E_z(\mathbf{k})$ must generate the same representation. The lowest combinations of powers of the components of $\mathbf{k}$ generating Γ_4 are

$$\begin{aligned}\kappa_x&=k_x(k_y^2-k_z^2) ,\\ \kappa_y&=k_y(k_z^2-k_x^2) ,\\ \kappa_z&=k_z(k_x^2-k_y^2) .\end{aligned} \tag{3}$$

Using this argument, Rashba and Sheka[8,9] showed that the expansion of $E(\mathbf{k})$ in powers of $\mathbf{k}$ gives an energy matrix of the form

$$E(\mathbf{k})=\frac{\hbar^2k^2}{2m^*}+\delta_0\boldsymbol{\sigma}\cdot\boldsymbol{\kappa}+\cdots , \tag{4}$$

where the constant δ_0 is a measure of the strength of the spin-orbit coupling for states in the conduction band. Note that we have written $\boldsymbol{\sigma}\cdot\boldsymbol{\kappa}=\sigma_x\kappa_x+\sigma_y\kappa_y+\sigma_z\kappa_z$ as a scalar product of two vectors. This notation is somewhat misleading because κ_x, κ_y, and κ_z do not form a vector or a pseudovector with respect to the three-dimensional orthogonal group. They are the components of a pseudovector within T_d. The notation in Eq. (4) is used as a convenient shorthand.

Besides k^4 there is only one independent invariant combination of fourth powers of components of $\mathbf{k}$, namely $k_y^2k_z^2+k_z^2k_x^2+k_x^2k_y^2$. Thus, taking terms to order four in $\mathbf{k}$, the energy eigenvalues of a Γ_6 band near $\mathbf{k}=0$ are obtained by diagonalizing

$$\begin{aligned}E(\mathbf{k})=&\frac{\hbar^2k^2}{2m^*}+\delta_0\boldsymbol{\sigma}\cdot\boldsymbol{\kappa}+\epsilon_0k^4\\ &+2\alpha_0(k_y^2k_z^2+k_z^2k_x^2+k_x^2k_y^2) .\end{aligned} \tag{5}$$

The quantities ϵ_0 and α_0 are phenomenological constants.

For convenience we introduce the functions $K(\hat{\mathbf{e}})$ and $M(\hat{\mathbf{e}})$ of an arbitrary unit vector $\hat{\mathbf{e}}$ defined by

$$K(\hat{\mathbf{e}})=e_y^2e_z^2+e_z^2e_x^2+e_x^2e_y^2 \tag{6}$$

and

$$M(\hat{\mathbf{e}})=[K(\hat{\mathbf{e}})-9e_x^2e_y^2e_z^2]^{1/2} , \tag{7}$$

where e_x, e_y, and e_z are the components of $\hat{\mathbf{e}}$ along the cubic axes. The extrema of $K(\hat{\mathbf{e}})$ are $\frac{1}{3}$, $\frac{1}{4}$, and 0 and occur along the $\langle 111\rangle$, $\langle 110\rangle$, and $\langle 100\rangle$ directions, respectively. The corresponding values of $M(\hat{\mathbf{e}})$ are 0, $\frac{1}{2}$ and 0, respectively. The electron energy levels, to fourth order in $\mathbf{k}=\hat{\mathbf{e}}k$, are

$$E_{\pm}=\frac{\hbar^2k^2}{2m^*}\pm\delta_0k^3M(\hat{\mathbf{e}})+[\epsilon_0+2\alpha_0K(\hat{\mathbf{e}})]k^4 . \tag{8}$$

The signs $\pm$ correspond to the orthogonal spin states

$$\chi_+=\left[|\uparrow\rangle\cos\frac{\theta}{2}+|\downarrow\rangle e^{i\phi}\sin\frac{\theta}{2}\right] ,$$

and

$$\chi_-=\left[-|\uparrow\rangle\sin\frac{\theta}{2}+|\downarrow\rangle e^{i\phi}\cos\frac{\theta}{2}\right] ,$$

where $|\uparrow\rangle$ and $|\downarrow\rangle$ are the spin-up and spin-down states referred to the [001] axis, $\cos\theta=M^{-1}e_z(e_x^2-e_y^2)$ and

$$\sin\theta e^{i\phi}=M^{-1}[e_x(e_y^2-e_z^2)+ie_y(e_z^2-e_x^2)] .$$

For example, for $\mathbf{k}$ parallel to the [110] direction

$$E_{\pm}(k)=\frac{\hbar^2k^2}{2m^*}\pm\tfrac{1}{2}\delta_0k^3+(\epsilon_0+\tfrac{1}{2}\alpha_0)k^4 . \tag{9}$$

The χ_+ and χ_- states are the eigenvectors of $\boldsymbol{\sigma}\cdot\hat{\mathbf{e}}_{\perp}$, where $\hat{\mathbf{e}}_{\perp}=2^{-1/2}(1,-1,0)$, i.e., the eigenvectors of the component of $\boldsymbol{\sigma}$ along $[1\bar{1}0]$. The sign of δ_0 determines the orientation of the spin in the lowest energy level for electrons having $\mathbf{k}$ vectors along $\langle 110\rangle$. Taking the origin of the cubic axes at an indium site and orienting the cubic axes so that an antimony atom lies along [111] at a distance $(a/4)\sqrt{3}$ from indium, with a the lattice constant, Cardona *et al.*[10] have shown that δ_0 is negative in InSb. Thus, in its lowest state, the spin of an electron with $\mathbf{k}$ along [110] is parallel to $[1\bar{1}0]$.

To derive the effective-mass Hamiltonian in the presence of a uniform magnetic field $\mathbf{B}_0=\nabla\times\mathbf{A}_0$ we replace $\mathbf{k}$ in $E(\mathbf{k})$ by the operator $-i\nabla+(e\mathbf{A}_0/\hbar c)$. The components of $\mathbf{k}$ do not now commute but rather they obey the relation

$$\mathbf{k}\times\mathbf{k}=-ie\mathbf{B}_0/\hbar c . \tag{10}$$

The Hamiltonian of a conduction electron near the center of the Brillouin zone in the presence of a magnetic field is[11]

$$H=H_0+H_1 , \tag{11}$$

where

$$H_0=\frac{\hbar^2k^2}{2m^*}+\tfrac{1}{2}g_0\mu_B\mathbf{B}_0\cdot\boldsymbol{\sigma} \tag{12}$$

and

$$\begin{aligned}H_1=&\delta_0\boldsymbol{\sigma}\cdot\boldsymbol{\kappa}+\epsilon_0k^4+\alpha_0(\{k_y^2,k_z^2\}+\{k_z^2,k_x^2\}+\{k_x^2,k_y^2\})\\ &+\beta_0\mu_B^2B_0^2+g'\mu_B\boldsymbol{\sigma}\cdot\mathbf{B}_0k^2+g''\mu_B\{\boldsymbol{\sigma}\cdot\mathbf{k},\mathbf{B}_0\cdot\mathbf{k}\}\\ &+\gamma_0\mu_B(\sigma_xB_{0x}k_x^2+\sigma_yB_{0y}k_y^2+\sigma_zB_{0z}k_z^2) .\end{aligned} \tag{13}$$

Here g_0 is the electron g factor in the limit of vanishing magnetic field and μ_B is the Bohr magneton. The symbol $\{u,v\}$ stands for the anticommutator $uv+vu$ and g', g'', γ_0, and β_0 are additional phenomenological constants required by symmetry. Here the expansion has been carried to the fourth power in k_x,k_y,k_z, and Eq. (13) is obtained after use of Eq. (10). The operators $\kappa_x,\kappa_y,\kappa_z$ are made Hermitian by symmetrizing their expressions in Eqs. (3).

The appropriate Hermitian forms are

$$\kappa_x = k_y k_x k_y - k_z k_x k_z \ , \qquad \kappa_y = k_z k_y k_z - k_x k_y k_x \ , \tag{14}$$

and

$$\kappa_z = k_x k_z k_x - k_y k_z k_y \ .$$

The eigenstates of H_0 are the ordinary spin-split Landau levels characterized by the following quantum numbers: $n=0,1,2,\ldots$, the Landau quantum number; k_ζ, the momentum along $\mathbf{B}_0$ in units of $\hbar$; M, the component of orbital angular momentum along $\mathbf{B}_0$; and $s=\pm\frac{1}{2}$, the intrinsic spin along $\mathbf{B}_0$.[12] In the presence of the perturbation H_1, the quantum numbers n, k_ζ, M, and s cease to be good quantum numbers. We denote the eigenvectors of H_0 by $|\nu\rangle$ instead of by $|n,k_\zeta,M,s\rangle$. The corresponding unperturbed eigenvalue is E_ν. The perturbed wave functions ψ_ν and their corresponding eigenvalues W_ν are obtained from the Schrödinger equation

$$(H_0+H_1)\psi_\nu = W_\nu \psi_\nu \ . \tag{15}$$

The energy eigenvalues are

$$W_\nu = E_\nu + \langle \nu | H_1 | \nu \rangle + \sum_{\nu'}{}' \frac{|\langle \nu | H_1 | \nu' \rangle|^2}{E_\nu - E_{\nu'}} + \cdots \ , \tag{16}$$

using standard second-order perturbation theory. We note that $\delta_0 \boldsymbol{\sigma}\cdot\boldsymbol{\kappa}$ is nondiagonal and thus contributes to the energy only in second order. The g factor is defined by

$$g\mu_B B_0 = W(n,k_\zeta,M,\tfrac{1}{2}) - W(n,k_\zeta,M,-\tfrac{1}{2}) \ . \tag{17}$$

Carrying out the operations implied in Eqs. (16) and (17) we obtain

$$g = g_0 + 4g' R_0^{-2}(n+\tfrac{1}{2}+\tfrac{1}{2}k_\zeta^2 R_0^2) + 4g'' k_\zeta^2 + 4\gamma_0 R_0^{-2}[(n+\tfrac{1}{2}-k_\zeta^2 R_0^2)K(\hat{\zeta}) + \tfrac{1}{2}k_\zeta^2 R_0^2] + \Delta g \ . \tag{18}$$

Here R_0 is the Landau length (the radius of the classical cyclotron orbit of energy $\frac{1}{2}\hbar\omega_c$),

$$R_0 = (\hbar c/eB_0)^{1/2} \tag{19}$$

and Δg the second-order contribution proportional to δ_0^2. The latter equals

$$\Delta g = -\delta_0^2 \frac{m^{*2} m \omega_c}{\hbar^5}\left[\left[\frac{6}{3-\mu}-\frac{1}{1+\mu}\right][\cos^2(2\alpha)\cos^2(2\beta)+\tfrac{1}{4}\sin^2(2\alpha)\cos^2\beta(1-3\cos^2\beta)] + \frac{9}{1-\mu}\sin^2(2\alpha)\sin^2(2\beta)\sin^2\beta\right] . \tag{20}$$

In this equation

$$\mu = g_0 m^*/2m \tag{21}$$

and β and α are the polar angles of $\hat{\zeta}$ (a unit vector parallel to $\mathbf{B}_0$) with respect to the cubic axes x,y,z. Using $\delta_0 = -2.2\times10^{-22}$ eV cm^3 $= -56$ a.u. (Refs. 10, 12, and 13), $m^* = 0.013m$, and $g_0 \approx -50$ for InSb we find that $\Delta g \sim 0.7\times10^{-3}$ at $B_0 = 4.15\times10^4$ G. Therefore, Δg can be neglected compared to the other terms. We note that g depends on the quantum numbers n and k_ζ and all the anisotropy is associated with the term in γ_0 as expected from the form of H_1. For the lowest Landau level ($n=0$, $k_\zeta=0$) we find

$$g = g_0 + 2g' R_0^{-2} + 2\gamma_0 R_0^{-2} K(\hat{\zeta}) \ . \tag{22}$$

The g factors determined in our measurements from the position of the spin-resonance line differ from g_0 (i.e., from the limiting value of g as B_0 tends to zero) by about 30%. Figures 1, 2, and 3 show the variation of the g factors as a function of the angle between the magnetic field $\mathbf{B}_0$ and the [100], [001], and [$\bar{1}$10] directions when $\mathbf{B}_0$ is confined to the (001), (110), and (112) planes, respectively. The data of Chen *et al.*[14] are shown in solid circles and the theoretical curves have been fit to the data with $g_0 = -51$, $g' = 6.0\times10^{-12}$ cm^2 $= 2.1\times10^5$ a.u., and $\gamma_0 = 8.2\times10^{-13}$ cm^2 $= 2.9\times10^4$ a.u.

The graph of $\mathbf{B}_0$ lying in the (111) plane was not

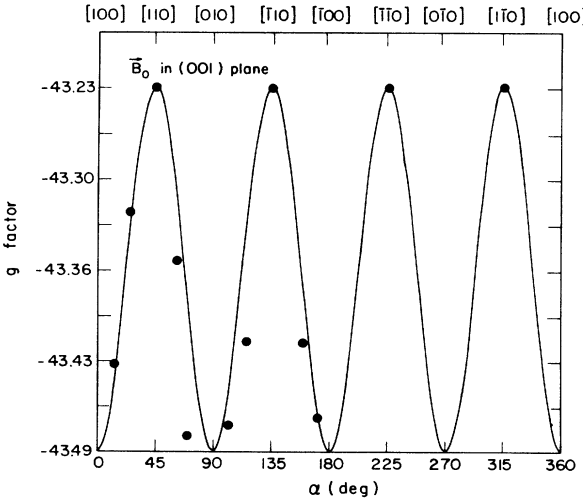

FIG. 1. g factor at the bottom of the conduction band of InSb as a function of the direction of the magnetic field $\mathbf{B}_0$ in the (001) plane. The intensity of $\mathbf{B}_0$ is at the position of the EDSR line for incident radiation of wavelength 118.8 μm. Liquid helium used as coolant. Experimental points taken from Chen *et al.* (Ref. 14). The solid line is the theoretical curve deduced from Eq. (22). The parameters g_0, g', and γ_0 were fitted to the data.

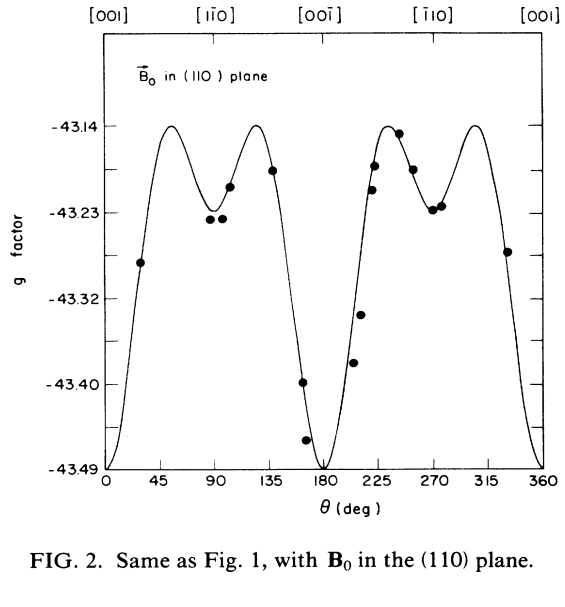

FIG. 2. Same as Fig. 1, with $\mathbf{B}_0$ in the (110) plane.

displayed because in this case g is isotropic; in fact, if $\mathbf{B}_0$ is in a (111) plane, $\zeta_x+\zeta_y+\zeta_z=0$; since $\hat{\xi}\cdot\hat{\xi}=1$, $\zeta_y\zeta_z+\zeta_z\zeta_x+\zeta_x\zeta_y=-\frac{1}{2}$; squaring this expression

$$K(\hat{\xi})+2\zeta_x\zeta_y\zeta_z(\zeta_x+\zeta_y+\zeta_z)=K(\hat{\xi})=\tfrac{1}{4}\ ,$$

the same for all directions of $\mathbf{B}_0$ in this plane.

We note that measurements of g for free electrons only yield values for the parameters g_0, g', and γ_0. However, the difference in the g factors for free and bound electrons allows us to determine g'', the only remaining relevant parameter in H_1. This is based on the following considerations.

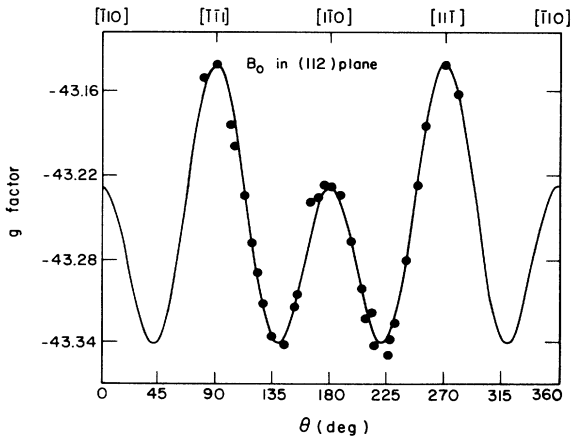

FIG. 3. Same as Fig. 1, with $\mathbf{B}_0$ in the (112) plane. Note that a (112) plane contains the directions [111] and [1$\bar{1}$0] but no cubic axes. Thus, the value of $K(\hat{\xi})=0$ is not attained when $\mathbf{B}_0$ is in a (112) plane. There is, however, an additional extremum of $K(\hat{\xi})$ subject to the restriction $\hat{\xi}\cdot[112]=0$. Then $K=\frac{1}{4}-\frac{3}{2}\zeta_z^2+\frac{21}{4}\zeta_z^4$ has a minimum for $|\zeta_z|=(1/\sqrt{7})$. One such direction is $[-(\sqrt{2}+1)/\sqrt{7},\ (\sqrt{2}-1)/\sqrt{7},\ (1/\sqrt{7})]$ forming an angle of 40.9° with [$\bar{1}$10].

The states of an electron bound to a donor are obtained solving the effective mass Schrödinger equation for the envelope function in the theory of shallow donors.[15] The effective mass Hamiltonian for the electron bound to an ionized donor is obtained adding to the Hamiltonian (11), the Coulomb potential screened by the dielectric constant ϵ,

$$H=H_0-\frac{e^2}{\epsilon r}+H_1\ , \tag{23}$$

where H_0 and H_1 are given by Eqs. (12) and (13). As before, we take H_1 as a perturbation. The eigenstates of the auxiliary Hamiltonian

$$K=\frac{\hbar^2k^2}{2m^*}-\frac{e^2}{\epsilon r} \tag{24}$$

are suitably scaled hydrogenic wave functions in which the unit of length is the effective Bohr radius $a^*=\epsilon\hbar^2/m^*e^2$ and the unit of energy is $m^*e^4/\hbar^2\epsilon^2$, twice the effective Rydberg. The term $\frac{1}{2}g_0\mu_B\mathbf{B}_0\cdot\boldsymbol{\sigma}=\frac{1}{2}g_0\mu_BB_0\sigma_\zeta$ has been dropped temporarily because, in the solution of the Schrödinger equation for $H_0-(e^2/\epsilon r)$, it does not affect the orbital part of the wave functions. When we consider the perturbations, this contribution to H will be restored.

With the units just mentioned, K can be written in the form

$$K=-\tfrac{1}{2}\nabla^2-\frac{1}{r}+\frac{\gamma}{2i}\left[\xi\frac{\partial}{\partial\eta}-\eta\frac{\partial}{\partial\xi}\right]+\frac{\gamma^2}{8}(\xi^2+\eta^2)\ , \tag{25}$$

where

$$\gamma=\left[\frac{a^*}{R_0}\right]^2\ . \tag{26}$$

Thus $\gamma^{-1/2}$ is a measure of the Landau radius in units of a^*. For $B_0=41.5\times10^3$ G and the parameters for InSb ($m^*=0.013m$, $\epsilon=16.8$, $a^*=7\times10^{-6}$ cm) we find $R_0=1.3\times10^{-6}$ cm and $\gamma=29$. This means that we cannot regard the terms involving γ in Eq. (25) as small. We note that K and L_ζ are commuting observables. Unfortunately the Schrödinger equation associated with the Hamiltonian K is not completely separable. Approximate solutions to this eigenvalue problem have been given by Elliott and Loudon,[16] Boyle and Howard,[17] and Baldereschi and Bassani,[18] who have calculated the energy eigenvalues. Accurate solutions can be found for $\gamma\ll1$ and $\gamma\gg1$. For the latter we attempt to find solutions of $K\psi=E\psi$ of the form

$$\psi=R_{nM}(\rho)(2\pi)^{-1/2}e^{iM\phi}\chi(\zeta,\rho)\ , \tag{27}$$

where ρ, ϕ, and ζ are cylindrical coordinates ($\xi+i\eta=\rho e^{i\phi}$). Here the function $R_{nM}(\rho)$ is the solution of the radial Schrödinger equation in cylindrical coordinates when we omit the Coulomb interaction. This is given by

$$R_{nM}(\rho)=C_{nM}e^{-(1/4)\gamma\rho^2}\rho^{|M|}F(\tfrac{1}{2}|M|+\tfrac{1}{2}M-n,|M|+1,\tfrac{1}{2}\gamma\rho^2)\ ,$$

where $F(a,c,z)$ is the confluent hypergeometric function and C_{nM} a normalization constant. The confluent hypergeometric function is defined by

$$F(a,c,z)=1+\frac{a}{c}z+\frac{a(a+1)}{2!c(c+1)}z^2+\cdots+\frac{a(a+1)\cdots(a+k-1)}{k!c(c+1)\cdots(c+k-1)}z^k+\cdots\ .$$

Some of the wave functions $R_{nM}(\rho)$ are

$$R_{00}(\rho)=\gamma^{1/2}\exp(-\gamma\rho^2/4)\ ,$$

$$R_{0,-1}(\rho)=(\gamma\rho/\sqrt{2})\exp(-\gamma\rho^2/4)\ ,$$

$$R_{10}(\rho)=\gamma^{1/2}(1-\tfrac{1}{2}\gamma\rho^2)\exp(-\gamma\rho^2/4)\ ,$$

$$R_{11}(\rho)=(\gamma/\sqrt{2})\exp(-\gamma\rho^2/4)\ .$$

The quantum numbers n and M have the ranges $n=0,1,2,\ldots$ and $M=-\infty,\ldots,-2,-1,0,1,2,\ldots,n$, respectively. Substitution of the wave function (27) into the Schrödinger equation for the Hamiltonian (25), multiplication by ρR_{nM}, integration over ρ from 0 to ∞, and one integration by parts yield

$$\int_0^\infty\left[-\frac{1}{2}\frac{\partial^2\chi}{\partial\zeta^2}-\frac{\chi}{(\rho^2+\zeta^2)^{1/2}}-[E-(n+\tfrac{1}{2})\gamma]\right]\rho R_{nM}^2\,d\rho=0\ . \quad (28)$$

For the ground state ($n=0$, $M=0$), $R_{00}(\rho)$ differs significantly from zero only for $\rho<\gamma^{-1/2}=R_0$. In our case $R_0\ll a^*$, so that we can approximate $\chi(\zeta,\rho)$ by $\chi(\zeta)=\chi(\zeta,\rho=0)$ and obtain the equation

$$-\frac{1}{2}\frac{d^2\chi}{d\zeta^2}+U_{00}(\zeta)\chi=\left[E-\frac{\gamma}{2}\right]\chi\ , \quad (29)$$

where

$$U_{00}(\zeta)=-\int_0^\infty\frac{R_{00}^2(\rho)\rho\,d\rho}{(\rho^2+\zeta^2)^{1/2}}=-\left[\frac{\pi\gamma}{2}\right]^{1/2}\exp(\tfrac{1}{2}\gamma\zeta^2)\operatorname{erfc}\left[\left[\frac{\gamma\zeta^2}{2}\right]^{1/2}\right]\ . \quad (30)$$

Here $\operatorname{erfc}(x)=(2/\sqrt{\pi})\int_x^\infty e^{-t^2}dt$ is the complementary error function.

The Schrödinger equation (29) has been solved numerically to find E and χ as a function of γ for several levels. We have also calculated the expectation value of k_ζ^2 in the lowest energy state as a function of γ. This result will be needed in the evaluation of the g factor and is displayed in Table I and in Fig. 4. The difference in energy between spin states resulting from this solution, taking into account the term $\frac{1}{2}g_0\mu_B\mathbf{B}_0\cdot\boldsymbol{\sigma}$ and the perturbation H_1 gives

$$g_b=g_0+2g'\langle k^2\rangle+2g''\langle k_\zeta^2\rangle+2\gamma_0(\zeta_x^2\langle k_x^2\rangle+\zeta_y^2\langle k_y^2\rangle+\zeta_z^2\langle k_z^2\rangle)\ . \quad (31)$$

This expression can be simplified when $\gamma\gg1$ because the wave functions are products of $\chi(\zeta)$ and $C_{nM}R_{nM}(\rho)e^{im\phi}$. In the ground state ($n=0$, $M=0$), we obtain

$$\langle k^2\rangle=\langle k_\zeta^2\rangle+\langle k_\xi^2+k_\eta^2\rangle=\langle k_\zeta^2\rangle+\frac{1}{R_0^2} \quad (32)$$

and

$$\langle k_x^2\rangle=\langle k_\zeta^2\rangle\zeta_x^2+\langle k_\xi^2\rangle\xi_x^2+\langle k_\eta^2\rangle\eta_x^2=\langle k_\zeta^2\rangle\zeta_x^2+\frac{1}{2R_0^2}(\xi_x^2+\eta_x^2)=\langle k_\zeta^2\rangle\zeta_x^2+\frac{1}{2R_0^2}(1-\zeta_x^2)\ , \quad (33)$$

with similar expressions for $\langle k_y^2\rangle$ and $\langle k_z^2\rangle$. Thus

$$g_b=g_0+2g'R_0^{-2}+2\gamma_0R_0^{-2}K(\hat{\zeta})+2\{g'+g''+\gamma_0[1-2K(\hat{\zeta})]\}\langle k_\zeta^2\rangle\ . \quad (34)$$

TABLE I. Energy of the ground state and value of $\langle k_\zeta^2\rangle$ as a function of $\gamma=(a^*/R_0)^2$. E is in effective Rydbergs and $\langle k_\zeta^2\rangle$ in atomic units.

γ	E	$\langle k_\zeta^2\rangle$
1.0	−0.3637	0.2583
10.0	6.6591	0.8620
20.0	15.6945	1.2115
30.0	25.0243	1.4692
40.0	34.4957	1.6826
50.0	44.0532	1.8657
60.0	53.6695	2.0275
70.0	63.3288	2.1751
80.0	73.0212	2.3062
90.0	82.7400	2.4370
100.0	92.4805	2.5437

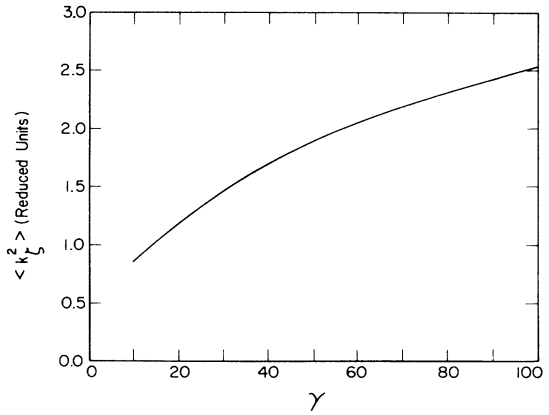

FIG. 4. Variation of $\langle k_\zeta^2\rangle$ with γ.

We note that the first three terms in Eq. (34) are formally identical to those for the lowest Landau level in the conduction band displayed in Eq. (22). Thus the difference in the g factors of the free and bound electron is given by the last term. There is, however, a small correction because the resonances do not occur at the same magnetic field. This means that in evaluating the contribution to g_b of the first three terms care must be taken to substitute the value of B_0 at the spin resonance for the bound electron.

III. EXPERIMENTAL PROCEDURE

Far-infrared magnetotransmission measurements were performed at liquid-helium temperature at a series of fixed wavelengths ($\lambda=96.5$, 118.8, 163, and 251.1 μm). The source of the radiation was an optically-pumped FIR laser, with CH_3OH as the lasing gas filling the FIR cavity. The samples were mounted in a Janis "supervaritemp" optical Dewar at the center of the split coil, 60-kG, superconducting solenoid. The temperature of the sample was monitored by a carbon-glass resistor placed next to it.

The transmitted FIR signal was detected by a carbon bolometer placed directly behind the sample. A lock-in amplifier with a 16-Hz chopper and an XY plotter were used to amplify and record the signal. The measurements were carried out in both the Voigt and the Faraday geometries, using linearly polarized waves in the former and circularly polarized waves (cyclotron-resonance-active and cyclotron-resonance-inactive, designated CRA and CRI, respectively) in the latter configuration.

The characteristics of the n-type InSb samples used in our experiments are given in Table II. Carrier concentrations were obtained from FIR Fabry-Perot oscillations.[19] Each sample was oriented by the standard Laue x-ray technique, cut on a diamond-wire saw such that the sample faces were parallel to a desired crystal plane, and then cut in the form of discs 7 mm in diameter. The surfaces of the disk samples were ground in succession with 600- and 1200-grit carborundum powder and then polished on a microcloth saturated with a suspension of 5-μm alumina powder in distilled water.

IV. EXPERIMENTAL RESULTS

An example of a typical magnetotransmission spectrum taken in the parallel Voigt geometry is shown in Fig. 5. The electric dipole spin resonance of conduction electrons is marked as EDSR in the figure. This normally electric-dipole-forbidden transition ($\Delta n=0$, $\Delta s=1$) is allowed in group-T_d crystals in the presence of spin-orbit coupling due to the lack of inversion symmetry.[13,20] The weaker sharp line which occurs at a lower magnetic field ($B_0=52.56$ kG) next to the conduction-electron EDSR is attributed to the spin-flip resonance of electrons bound to donors.

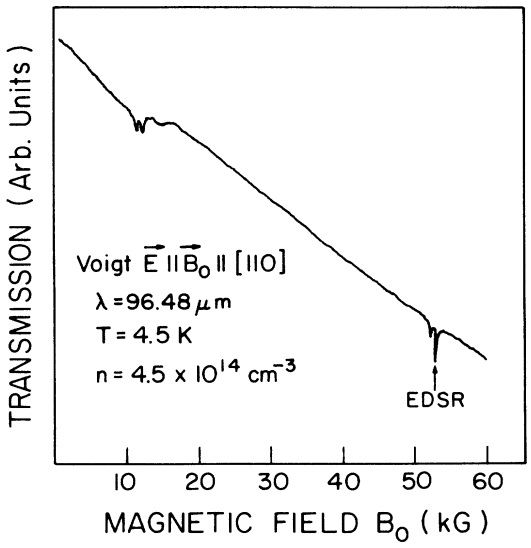

FIG. 5. Typical FIR magnetotransmission spectrum for the parallel Voigt ($\mathbf{E}||\mathbf{B}_0$) configuration obtained on sample No. 4 at 4.5 K and 96.48 μm, showing the EDSR of conduction electrons (marked in the figure), and the weaker line due to donor-bound electrons (next to EDSR). The features occurring at low fields were identified as combined resonances of conduction and donor-bound electrons, and are not discussed in this paper.

TABLE II. Sample parameters.

Sample number	Donor concentration (cm^{-3})	Thickness (mm)	Sample orientation
1	1.6×10^{14}	1.07	(112)
2	2.3×10^{14}	4.52	(110)
3	3.6×10^{14}	3.95	(100)
4	4.5×10^{14}	3.94	(111)
5	9.0×10^{14}	2.49	(112)

The spin-flip transitions of interest are shown schematically in Fig. 6. Our identification of the donor resonance is supported by the study of the dependence of this absorption line on the temperature, on donor concentration, and on the magnetic field. Comparison of the intensities of both the free-carrier and the donor resonances, measured at low temperatures in the parallel Voigt ($\mathbf{E}||\mathbf{B}_0$) geometry, is presented in Fig. 7. As can be seen in the figure, the intensity of the lower-magnetic-field peak decreases as the temperature increases, due to the ionization of the donors. It disappears at 12 K.

We have studied all the samples listed in Table II at $T=4.5$ K and we have found that the intensity of the lower-magnetic-field line decreases with respect to the higher-field line as the donor concentration increases. Examples from this study are presented in Fig. 8. As the donor concentration is increased, the width of the donor levels increases (due to interdonor perturbation), thus decreasing the ionization energy for the donors. As this "smearing" effect increases with increasing donor concentration, less and less energy is required to thermally ionize electrons from the donor levels to the $n=0$ Landau level of the conduction band.[20] This in turn will decrease the impurity-related spin-resonance intensity. Eventually, at

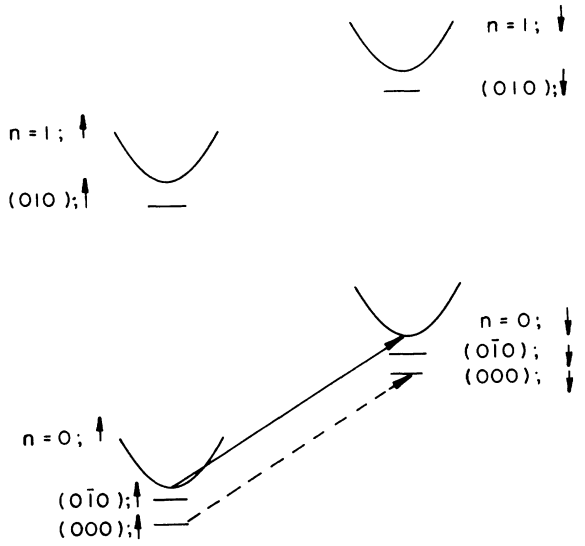

FIG. 6. A schematic representation of the energy levels of free and localized electrons in InSb in the high-field case. The lowest two Landau levels for both spin orientations are indicated by parabolas. Impurity states are identified using the notation of Ref. 11. The free-electron spin resonance transition is shown by a solid arrow, and the spin resonance of donor electrons by the dashed arrow. The energy levels are not drawn to scale.

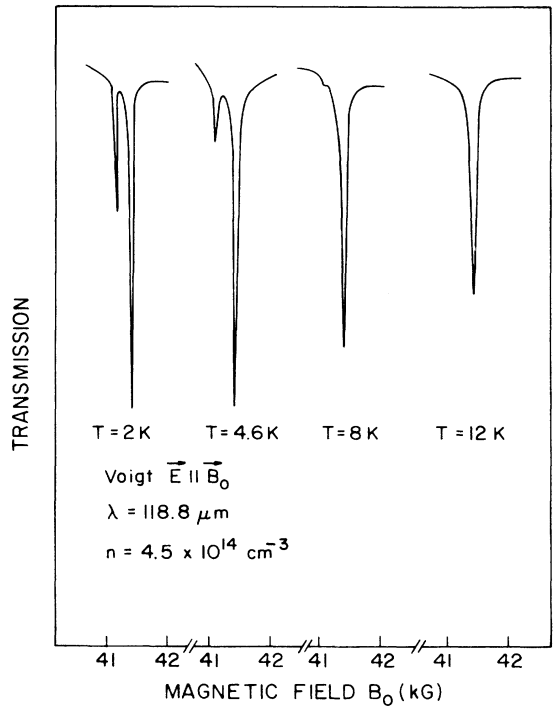

FIG. 7. EDSR spectra in the parallel Voigt geometry vs magnetic field, obtained on sample 4 for different temperatures. The stronger line is the free-electron EDSR, and the weaker line is EDSR of donor-bound electrons. Note that the intensity of the donor spin-flip transition clearly decreases with increasing temperature.

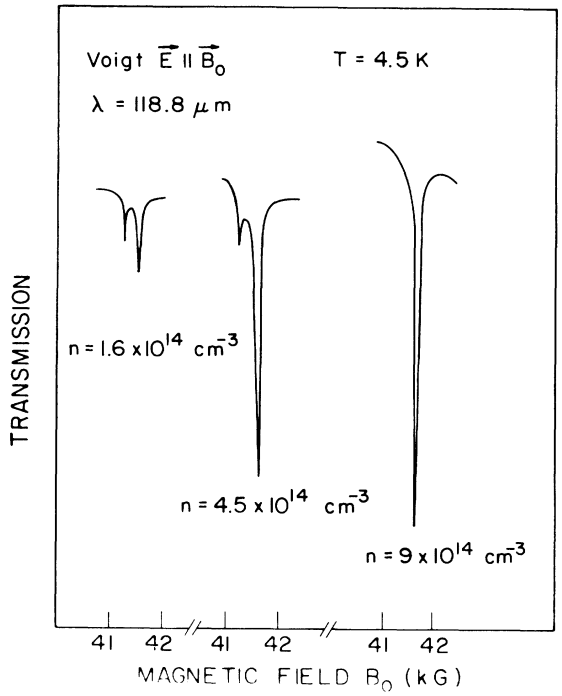

FIG. 8. EDSR spectra obtained in the parallel Voigt geometry vs magnetic field obtained at 4.5 K and 118.8 μm samples with different donor concentrations n. Note that the intensity of the donor EDSR decreases, and ultimately disappears, as the donor concentration is increased.

some value of donor concentration, the impurity levels will be sufficiently broad to merge with the conduction band (forming a low-energy tail connected to the bottom of the band), and the donor-related transitions will disappear altogether.

Finally, magnetic field dependence of the EDSR spectrum is shown in Fig. 9. As the magnetic field is increased, this increases the "magnetic freezeout" of the free electrons onto impurity states, and hence increases the transition intensity of donor electrons with respect to the intensity of the free-electron line.

According to the recent calculation of Wlasak[21] the mechanism allowing the electric-dipole-induced spin-flip resonance of donor-bound electrons in the parallel-Voigt geometry is the lack of inversion symmetry. The angular dependence of the matrix elements for this transition given in Ref. 20 is identical with the angular dependence for EDSR of conduction electrons.[13,12] In Fig. 10 we compare the spin-resonance absorption coefficients for free and donor-bound electrons observed at 118.8 μm in the parallel Voigt geometry as a function of orientation of $\mathbf{B}_0$ in the (111) plane (sample No. 3 in Table II). Note that the strong angular dependence of the data is identical for both types of electrons. Note also that there is a difference in the absorption coefficient (by a factor of about 2) between the [011] direction and the equivalent [110] and [$\bar{1}$01] directions. This is the recently discovered effect of the electric-dipole—magnetic-dipole interfer-

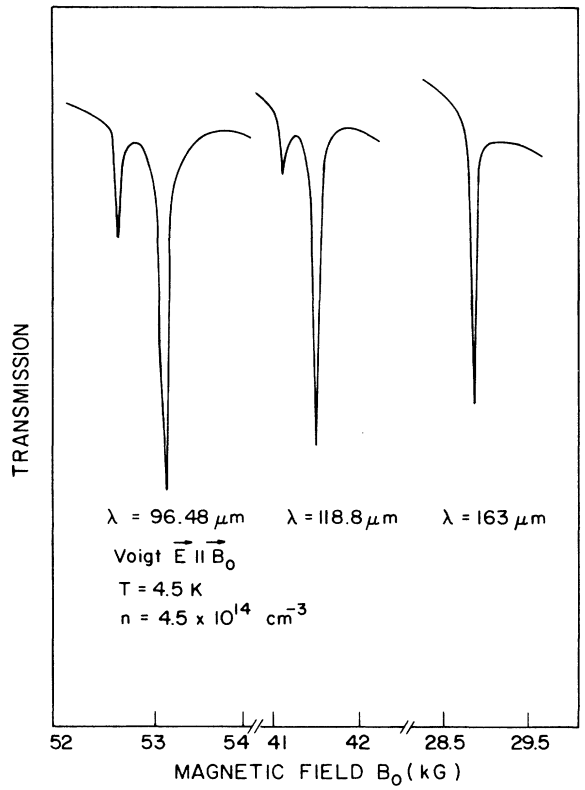

FIG. 9. EDSR spectra obtained in the parallel Voigt geometry vs magnetic field observed on sample 4 at 4.5 K for different laser frequencies. Note that the intensity of the donor EDSR increases with magnetic field, due to the fact that as the field increases the donor sites are increasingly populated by the freeze-out mechanism.

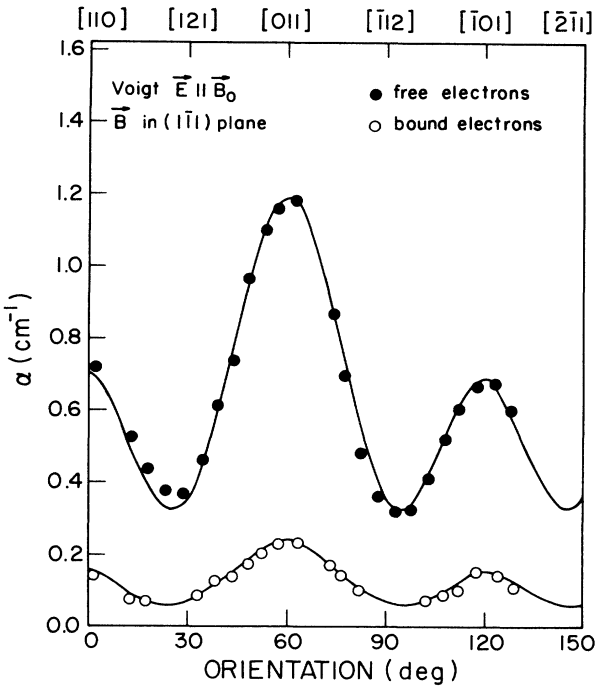

FIG. 10. Spin resonance absorption coefficient of conduction electrons (solid circles) and donor electrons (open circles) in *n*-InSb for the parallel Voigt geometry as a function of orientation of $\mathbf{B}_0$ in the $(1\bar{1}1)$ plane. The data were taken on sample No. 4 at 118.8 μm and 4.5 K. The upper solid line is the theoretical angular dependence fitted to the experimental data. The lower solid curve is a guide for the eyes.

ence.[12,13] This effect was described in Refs. 13 and 12 for the free-electron spin resonance, and it is important to note that it applies equally well to donor electrons. The upper solid line in Fig. 10 is calculated theoretically for free electrons by adjusting the magnitude of the electric-dipole and magnetic-dipole resonance intensities.[13,12] The lower line is a guide for the eye. Note, however, that it reflects exactly the behavior of the upper (i.e., the free electron) curve, indicating that both the electric dipole and the magnetic dipole matrix elements contribute to the spin-flip transitions of bound electrons. The calculations for the electric-dipole—magnetic-dipole interference for bound electrons are in progress and will be published later.

The ability to observe EDSR in the parallel Voigt geometry is particularly gratifying, since this configuration is ideally suited for carrying out measurements of the anisotropy of the g factor. The g-factor anisotropy of conduction electrons has been analyzed in the paper of Chen *et al.*[14] The g factor for the donor electrons can be determined very precisely using the expression (17) equated to $\hbar\omega$ where ω is the FIR angular frequency.

In order to determine the value and the complete angular dependence of the g factor of donor electrons, we have examined its anisotropy through 360° in the parallel Voigt geometry for $\mathbf{B}_0$ in the (100), (110), (111), and (112) planes. We have found that for every plane the g-factor anisotropy of donor electrons is, within the experimental error, exactly the same as for the free electrons, and that the difference between the g-factor values for the free and donor-bound electrons, $\Delta = g_b - g_c$, is constant for any given FIR frequency within the experimental accuracy. For example, $\Delta = -0.380 \pm 0.015$ for $\lambda = 118.8$ μm for every crystallographic plane examined. This result is presented in Fig. 11, showing the dependence of both g factors on the angle between the direction of $\mathbf{B}_0$, and the crystallographic axis for the (110) plane. The solid circles and open circles in the figure are experimental data observed at 4.5 K and 118.8 μm. The solid circles were obtained in the parallel Voigt geometry on sample 2. The triangles are from data observed on sample 3 in the CRA geometry for $\mathbf{B}_0 \| [100]$ and $\mathbf{B}_0 \| [111]$, since for these precise orientations EDSR disappears in the parallel Voigt geometry. The solid curves in Fig. 11 are a guide for the eye. Unfortunately we were not able to observe the spin resonance of donor electrons in the Faraday geometry because, as seen for free electrons, in this configuration the intensity of EDSR is approximately 10 times weaker than that for the parallel Voigt geometry.[13]

Our measurements were carried out with incident radia-

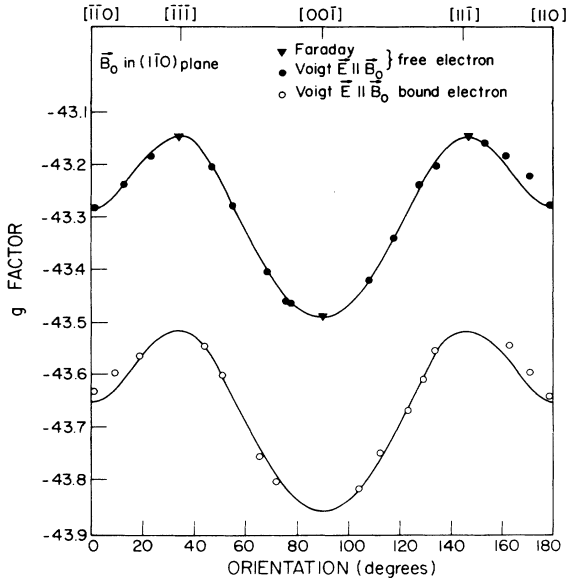

FIG. 11. Effective g factor as a function of orientation of $\mathbf{B}_0$ in the (110) plane for conduction electrons (solid circles and triangles) and electrons bound to donors (open circles). The points are experimental: the solid circles and open circles were observed in the parallel Voigt geometry on sample 2; the triangles were observed on sample 3 in the CRA geometry ($\mathbf{B}_0 \| [100]$) and on sample 4 in the CRI geometry ($\mathbf{B}_0 \| [111]$). All experimental data were taken at 118.8 μm at 4.5 K. The solid lines are a guide for the eyes.

tion of wavelengths $\lambda=118.8$ μm and $\lambda=96.48$ μm. For the first, the spin-flip resonances occurred at $B_{01}=41.5\times10^3$ G for free electrons and at $B_{02}=41.14\times10^3$ G for electrons bound to donors. The corresponding values when $\lambda=96.48$ μm were $B_{01}=53.095\times10^3$ G and $B_{02}=52.56\times10^3$ G. The parameter γ defined by Eq. (26) has the values $\gamma_1=29.54$ and $\gamma_2=29.28$ at the resonance positions for $\lambda=118.8$ μm. When $\lambda=96.48$ μm the corresponding values of γ are $\gamma_1=37.73$ and $\gamma_2=37.41$. According to the results of Sec. II the difference Δ between the values g_b and g_c at the free electron resonance is

$$\Delta=2(m^*/\epsilon m)^2[\Delta\gamma g'+(g'+g''+\gamma_0)\langle k_\zeta^2\rangle +\gamma_0(\Delta\gamma-2\langle k_\zeta^2\rangle)K(\hat{\zeta})], \quad (35)$$

where $\Delta\gamma=\gamma_2-\gamma_1$ and all quantities are expressed in atomic units. For $\gamma=29.28$, $\langle k_\zeta^2\rangle=1.45$; using the values of g' and γ_0 determined previously and the experimental result for $\mathbf{B}_0$ in a (110) plane, $\Delta\cong-0.380$, we obtain $g''=-4.2\times10^5$ a.u. The anisotropic term, proportional to $K(\hat{\zeta})$, contributes an amount -0.109 $K(\zeta)$ to this difference. Since the largest value of $K(\hat{\zeta})$ for $\mathbf{B}_0$ in a (110) plane is 0.25 this term contributes at most 0.0273 to Δ. Since the total margin of experimental error in Δ is 0.03 we are not able to determine the contribution to Δ of this anisotropic term. For $\gamma=37.41$, corresponding to the donor spin resonance for incident radiation of wavelength 96.48 μm, $\langle k_\zeta^2\rangle=1.63$. The difference Δ is, then, approximately -0.427 which compares favorably with the experimental value of -0.428. We note that the value of g'' obtained here is negative, as expected, but differs by 1 order of magnitude from that estimated by Ogg.[11] The nature of this discrepancy will be the object of a separate study.

V. CONCLUDING REMARKS

In summary, we have established the following points.

(a) We have shown that in the observed spin resonance doublet the line occurring at the lower field is due to donor-bound electrons. This has been demonstrated by a systematic study of the dependence of the spin resonance absorption on temperature, magnetic field, and donor concentration.

(b) The behavior of the spin resonance intensity for donor-bound electrons is the same (i.e., the same dependence on the orientation of $\mathbf{B}_0$ relative to the crystal axes, and the same electric-dipole-magnetic-dipole interference) as for conduction electrons. This is to be expected, because for $\gamma\gg1$ the nature of the wave functions in the plane perpendicular to $\mathbf{B}_0$ is the same for both cases.

(c) The g-factor anisotropy of the donor is also observed to be the same as that for conduction electrons. The small anisotropy in Δ proportional to γ_0 is apparently smaller than the margin of error in our experiment.

(d) We formulate a theoretical model which correctly predicts the value of $\Delta=g_b-g_c$. By fitting our experimental data to the model, we have obtained the parameters g_0, g', γ_0, and g'', which completely describe the effective g factor for donor-bound electrons in InSb.

(e) Our theory also predicts a frequency dependence for Δ, which agrees with experiment in our FIR frequency range. Inspection of the model indicates that for lower photon energies ($\gamma\lesssim1$) the donor spin-resonance line should appear at fields *above* the conduction-electron spin resonance. This may account for the behavior of spin resonance data in InSb reported by Appold *et al.*[7] A systematic extension of spin resonance measurements to energies $\hbar\omega<7$ meV should thus be extremely valuable.

ACKNOWLEDGMENTS

The authors are grateful to Dr. Y.-F. Chen for his contributions to a part of the experimental work and for valuable discussions. This work was supported by the National Science Foundation (Grants No. DMR 86-00014, DMR 84-18453, and INT 81-03336).

*Present address: Facultad de Fisica, Pontificia Universidad Católica de Chile, Casilla 6177, Santiago, Chile.

†Permanent address: Worcester Polytechnic Institute, Worcester, Massachusetts 01609.

[1]R. Kaplan, Phys. Rev. **181**, 1154 (1969).

[2]R. Kaplan, R. A. Cooke, and R. A. Stradling, Solid State Commun. **26**, 741 (1978).

[3]L. E. Blagoskonskaya, E. M. Gershenson, G. N. Goltsman, and

A. I. Elantev, Fiz. Tekh. **11**, 2373 (1977) [Sov. Phys.—Semicond. **11**, 1395 (1977)].

[4]B. D. McCombe and R. Kaplan, Phys. Rev. Lett. **21**, 756 (1968).

[5]W. Zawadzki and J. Wlasak, *Theoretical Aspects and New Developments in Magneto-Optics,* edited by J. T. Devreese (Plenum, New York, 1980), p. 347.

[6]B. D. McCombe and R. J. Wagner, in *Proceedings of the 11th Conference on the Physics of Semiconductors,* edited by M. Miasek (Polish Scientific Publishers, Warsaw, 1972), p. 321.

[7]G. Appold, H. Pasher, R. Ebert, U. Steigenberger, and K. von Ortenberg, Phys. Status Solidi B **86**, 557 (1978).

[8]E. I. Rashba and V. I. Sheka, Fiz. Tverd. Tela (Leningrad) **3**, 1973 (1961) [Sov. Phys.—Solid State **3**, 1257 (1961)].

[9]E. I. Rashba and V. I. Sheka, Fiz. Tverd. Tela (Leningrad) **3**, 1836 (1961) [Sov. Phys.—Solid State **3**, 1357 (1961)].

[10]M. Cardona, N. E. Christensen, M. Dobrowolska, J. K. Furdyna, and S. Rodriguez, Solid State Commun. **60**, 17 (1986).

[11]N. R. Ogg, Proc. Phys. Soc. **89**, 431 (1966).

[12]See, for example, S. Gopalan, J. K. Furdyna, and S. Rodriguez, Phys. Rev. B **32**, 903 (1985).

[13]Y.-F. Chen, M. Dobrowolska, J. K. Furdyna, and S. Rodriguez, Phys. Rev. B **32**, 890 (1985).

[14]Y.-F. Chen, M. Dobrowolska, and J. K. Furdyna, Phys. Rev. B **31**, 7989 (1985).

[15]See, for example, A. K. Ramdas and S. Rodriguez, Rep. Prog. Phys. **44**, 1297 (1981).

[16]R. J. Elliot and R. Loudon, J. Phys. Chem. Solids **15**, 196 (1960).

[17]W. S. Boyle and R. E. Howard, J. Phys. Chem. Solids **19**, 181 (1961).

[18]A. Baldereschi and F. Bassani, in *Proceedings of the 10th International Conference on the Physics of Semiconductors, Cambridge, Massachusetts,* edited by S. P. Keller, J. C. Hensel, and F. Stern (USAEC Division of Technical Information, Washington, D.C., 1970), p. 191.

[19]Y.-F. Chen, Ph.D. thesis, Purdue University, 1984 (unpublished).

[20]F. Kuchar, E. Fantner, and G. Bauer, J. Phys. C **10**, 3577 (1977).

[21]J. Wlasak, J. Phys. C **18**, 4001 (1985).